Structure of elementary excitations and temperature dependence of the momentum distribution in liquid ^{4}He

E. Manousakis and V. R. Pandharipande
Department of Physics and Materials Research Laboratory, University of Illinois at Urbana—Champaign, 1110 W. Green Street, Urbana, Illinois 61801
(Received 17 December 1984)

We study the momentum-space structure of the elementary excitations in liquid ^{4}He by calculating the change $\delta n_{\mathbf{k}}(\mathbf{p})$ in the momentum distribution of atoms on creating an excitation of momentum $\mathbf{k}$. Jastrow and Jastrow plus triplet wave functions are used for the ground state, and the excitations are created with Feynman and Feynman-Cohen excitation operators. We find that the excitations in the long-wavelength limit are harmonic vibrations with equal amount of change in kinetic and potential terms. At large k, however, they become "single-particle"-like; and most of the energy comes from removing one particle from the ground-state momentum distribution and putting it at states with $\mathbf{p}\sim\mathbf{k}$. The $\delta n_{\mathbf{k}}(\mathbf{p})$ is used to calculate the momentum distribution $n(T,p)$ of the liquid at low temperatures (<1 K). The temperature dependence of the fraction of atoms in the $p=0$ condensate and the $1/p^2$ and $1/p$ singularities of $n(T,p)$ are discussed.

I. INTRODUCTION

The aim of this paper is to study the momentum-space structure of elementary excitations in liquid ^{4}He. The momentum distribution $n_0(p)$ of the atoms in the ground state of liquid ^{4}He has been studied by the Green's-function Monte Carlo[1,2] (GFMC) and variational[3,4] methods. The initial variational calculations[3] used the Jastrow (J) wave function:

$$\Psi_0=\Omega^{-N/2}\prod_{i<j}f(r_{ij})\ , \tag{1.1}$$

for the ground state. Here Ω is the normalization volume and N is the number of particles. The thermodynamic limit $N\to\infty$, $\Omega\to\infty$ at fixed density $\rho=N/\Omega$ is assumed. Recently we[4] calculated the $n_0(p)$ with a more realistic wave function, which contains optimized Jastrow and three-body [Jastrow plus triplet (J + T)] correlations:

$$\Psi_0=\Omega^{-N/2}\sum_{i<j}f(r_{ij})\prod_{i<j<k}f_3(r_{ij},r_{jk},r_{ki})\ . \tag{1.2}$$

The GFMC and variational $n_0(p)$ are in reasonable agreement with each other and the experimental data.[5,6]

In this work we consider the change $\delta n_{\mathbf{k}}(\mathbf{p})$ in the momentum distribution of atoms due to an elementary excitation of momentum $\mathbf{k}$. The wave functions and spectra of elementary excitations in liquid ^{4}He have been studied by many authors. The first approximation for the wave function of an excitation of momentum $\mathbf{k}$ is Feynman's:

$$\Psi_{\mathbf{k}}=\rho_F(\mathbf{k})\Psi_0\ , \tag{1.3}$$

$$\rho_F(\mathbf{k})=\sum_{i=1}^{N}e^{i\mathbf{k}\cdot\mathbf{r}_i}\ . \tag{1.4}$$

An improved wave function,

$$\Psi_{\mathbf{k}}=\rho_B(\mathbf{k})\Psi_0\ , \tag{1.5}$$

$$\rho_B(\mathbf{k})=\sum_{i=1}^{N}e^{i\mathbf{k}\cdot\mathbf{r}_i}\left[1+i\sum_{j\neq i}\eta(r_{ij})\mathbf{k}\cdot\mathbf{r}_{ij}\right]\ , \tag{1.6}$$

was proposed by Feynman and Cohen[7] to account for the backflow current. We[8] have recently carried out detailed variational calculations of the spectrum of elementary excitations with the $\rho_B(\mathbf{k})$ and the J + T Ψ_0. A brief review of the earlier work on the wave functions and the spectrum of excitations in liquid ^{4}He is also given in Ref. 8. The energies obtained with these wave functions are satisfactory for the phonons, but they are $\sim$20% too high for the maxons and rotons. We developed a perturbation expansion using correlated basis functions (CBF) generated by the $\rho_B(\mathbf{k})$ operators. The second-order corrections to the spectrum improve the agreement with experiment very significantly.

In the next section we calculate the $\delta n_{\mathbf{k}}(\mathbf{p})$ using the Jastrow Ψ_0 and the Feynman $\rho_F(\mathbf{k})$. The general structure of $\delta n_{\mathbf{k}}(\mathbf{p})$ is discussed in detail, and the small and large k limits are calculated analytically. In Secs. III and IV we introduce the effects of the three-body and backflow correlations, respectively. At very low temperatures ($T<1$ K) the liquid can be described as low-density gas of excitations. In this limit we can use the $\delta n_{\mathbf{k}}(\mathbf{p})$ to study the low-temperature behavior of the momentum distribution of atoms in the liquid. This calculation is described in Sec. V.

II. CALCULATIONS WITH FEYNMAN-JASTROW WAVE FUNCTIONS

The $\delta n_{\mathbf{k}}(\mathbf{p})$ is given by

$$\begin{aligned}\delta n_{\mathbf{k}}(\mathbf{p})&=n_{\mathbf{k}}(\mathbf{p})-n_0(\mathbf{p})\\&=\int d^3r_{11'}[n_{\mathbf{k}}(\mathbf{r}_{11'})-n_0(\mathbf{r}_{11'})]e^{-i\mathbf{p}\cdot\mathbf{r}_{11'}}\ ,\end{aligned} \tag{2.1}$$

where $n_x(\mathbf{r}_{11'})$ is the one-body density matrix in the state $x=0,\mathbf{k}$:

$$n_x(\mathbf{r}_{11'})=\frac{N\int \Psi_x^*(1',2,\ldots,N)\Psi_x(1,2,\ldots,N)d^3r_2\cdots d^2r_N}{\int |\Psi(1,2,\ldots,N)|^2 d^3r_1\cdots d^3r_N}, \tag{2.2}$$

normalized so that

$$\frac{\Omega}{(2\pi)^3}\int n_x(\mathbf{p})d^3p=N .$$

Both $n_k(\mathbf{p})$ and $n_0(p)$ are of order 1, and the difference $\delta n_k(\mathbf{p})$ is of order $1/N$.

In this section we calculate the $\delta n_k(\mathbf{p})$ using Jastrow's approximation for the Ψ_0 [Eq. (1.1)], and the Feynman wave function [Eq. (1.3)] for the Ψ_k. The cluster expansion of $\delta n_k(\mathbf{p})$ is carried out in Sec. II A. The small- and large-k limits are calculated in Sec. II B, and the methods used for numerical calculations are discussed in Sec. II C.

A. Cluster expansion

We use the diagrammatic method developed for nuclear matter[9] to calculate the cluster expansion of $\delta n_k(\mathbf{p})$. Fantoni's[3] calculation of $n_0(p)$ is repeated by using methods of Ref. 9. The cluster expansion of $n_0(r_{11'})$ is obtained by expanding the numerator of $n_0(r_{11'})$ in powers of the functions:

$$h(r_{ij})=f^2(r_{ij})-1,\quad i,j\neq 1,1' \tag{2.3}$$

$$\zeta(r_{mj})=f(r_{mj})-1,\quad m=1,1' . \tag{2.4}$$

The integrals of this expansion are represented by diagrams which contain external points 1 and 1' and any number of internal points denoting particle coordinates to be integrated. The functions $h(r_{ij})$ and $\zeta(r_{mj})$ are represented by lines joining the points ij and mj. We obtain

$$\begin{aligned} Y_0\equiv N\int \Psi_0(\mathbf{r}_{1'},\mathbf{r}_2,\ldots,\mathbf{r}_N)&\\ \times\Psi_0(\mathbf{r}_1,\mathbf{r}_2,\ldots,\mathbf{r}_N)d^3r_2\cdots d^3r_N&\\ =\rho\{[I]+[I][i]+\tfrac{1}{2}[I][i][j]+\cdots\}&, \end{aligned} \tag{2.5}$$

where $[I]$ denotes a connected diagram having the points 1 and 1', and $[i]$, $[j]$, etc., denote connected diagrams having only h-lines. The products $[I][I]$, $[i][i][j]$, etc., represent disconnected diagrams. A sum over all diagrams $I,i,j,\ldots$, is implied with the constraint that the diagrams $I,i,j\cdots$, in the disconnected diagram $[I][i][j]\cdots$ have no common particles. Thus the product $[I]\times[i]\neq[I][i]$, since the product contains terms in which I and i have common particles.

The denominator is expanded in powers of h only, and we obtain

$$X_0\equiv\int \Psi_0^2(r_1,\ldots,r_N)d^3r_1\cdots d^3r_N =1+[i]+\tfrac{1}{2}[i][j]+\cdots . \tag{2.6}$$

On performing the division[9] we get

$$\begin{aligned} n_0(r_{11'})=\rho\{[I]-\overbrace{[I][i]}-\overbrace{[I][i]}-\cdots+\overbrace{[I][i][j]}&\\ +\tfrac{1}{2}\overbrace{[I][i][j]}+\overbrace{[I][i][j]}+\cdots-\cdots\}&. \end{aligned} \tag{2.7}$$

Here overhead bars denote common particles. For example $\overbrace{[I][i]}$ is the sum of the products of all diagrams I and i that have one common particle. The diagrams I and i contributing to $\overbrace{\overbrace{[I][i]}}$ must have two common particles, while only the diagrams I, i, and j that have one common particle contribute to $\overbrace{[I][i][j]}$, etc. The order of magnitude of the contribution of a term in Eq. (2.7) is given by N to power {the number of [ ] -1 $-$number of $\frown$ lines $-2\times$number of $\frown\!\frown$ lines $-\cdots$}. Thus $\overbrace{\overbrace{[I][i]}}$ has a contribution of order N^{-1}, and it is neglected while calculating the $n_0(p)$.

Compact cluster expansions are obtained by noting that the connected diagrams $[I]$ and $[i]$ can be expressed as

$$[I]=[A]+\overbrace{[Aa']}+\tfrac{1}{2}\overbrace{[Aa'b']}+\tfrac{1}{2}\overbrace{[Aa'b']}+\overbrace{[Aa'b']}+\cdots , \tag{2.8}$$

$$[i]=[a]+\tfrac{1}{2}\overbrace{[ab]}+\cdots , \tag{2.9}$$

where A denotes irreducible diagrams which contain both points 1 and 1'; and $a',b',\ldots,$ denote irreducible diagrams that may contain one or none of the points 1 and 1'. The term $\overbrace{[Aa']}$ represents all the diagrams in $[I]$ with one articulation point. $\overbrace{[Aa'b']}$ is the sum of diagrams that can be broken into three pieces at one articulation point, while $\overbrace{[Aa'b']}$ and $\overbrace{[Aa'b']}$ are sums of diagrams with two articulation points etc. The irreducible diagrams $a,b,\ldots,$ that occur in the expansion of $[i]$ are identical to the diagrams $a',b',\ldots,$ when they do not include the point 1 or 1'. Diagrams $a',b',\ldots,$ that include the point 1 or 1', are formed with ζ-lines starting from 1 or 1'; whereas diagrams $a,b,\ldots,$ which include the point 1 can come only from the $[i]$ in denominator, and they have only h-lines. The $a,b,\ldots,$ cannot have point 1'.

On substituting Eqs. (2.8) and (2.9) in Eq. (2.7) we obtain

$$\begin{aligned} \frac{1}{\rho}n_0(\mathbf{r}_{11'})=[A]+\{\overbrace{[Aa']}-\overbrace{[A][a]}\}+\{\tfrac{1}{2}\overbrace{[Aa'b']}-\overbrace{[Aa'][b]}-\tfrac{1}{2}\overbrace{[A][ab]}+\overbrace{[A][a][b]}\}&\\ +\{\tfrac{1}{2}\overbrace{[Aa'b']}-\overbrace{[Aa'][b]}+\tfrac{1}{2}\overbrace{[A][a][b]}\}+\{\overbrace{[Aa'b']}-\overbrace{[Aa'][b]}-\overbrace{[A][ab]}+\overbrace{[A][a][b]}\}+\cdots&. \end{aligned} \tag{2.10}$$

It can be easily verified that all the terms in the { } are zero unless the common points are 1 and/or 1'. Let $[a_1']$ and $[a_1]$ be the sums of irreducible a' and a diagrams with points 1, and $[a_{1'}']$ be the sum of irreducible diagrams with point 1'. The R_w and R_d of Ref. 3 are defined as

$$R_w=[a_1']=[a_{1'}'] , \tag{2.11}$$

$$R_d=[a_1]\ . \tag{2.12}$$

The sum $[A]$ can be factored out of the $n_0(r_{11'})$ to obtain

$$n_0(r_{11'})=\rho[A][1+2R_w-R_d+\tfrac{1}{2}(2R_w-R_d)^2+\cdots]\ . \tag{2.13}$$

The higher terms simply complete the exponential series, and we obtain the well-known[3] expression:

$$n_0(r_{11'})=\rho[A]\exp(2R_w-R_d)\equiv\rho[A]n_c\ , \tag{2.14}$$

where n_c is the fraction of particles in the $p=0$ condensate.

The cluster expansion of $\delta n_k(\mathbf{r}_{11'})$ is calculated in the same way. We express $\delta n_k(\mathbf{r}_{11'})$ as

$$\delta n_k(\mathbf{r}_{11'})=\frac{X_0}{X_k}\left[\frac{Y_k}{X_0}-\frac{Y_0}{X_0}\frac{X_k}{X_0}\right]\equiv\frac{X_0}{X_k}U_k\ , \tag{2.15}$$

$$Y_k=N\int\sum_{m,n}e^{i\mathbf{k}\cdot\mathbf{r}_{mn}}\Psi_0(\mathbf{r}_{1'},\ldots,\mathbf{r}_N)\times\Psi_0(\mathbf{r}_1,\ldots,\mathbf{r}_N)d^3r_2\cdots d^3r_N\ , \tag{2.16}$$

$$X_k=\int\sum_{m,n}e^{i\mathbf{k}\cdot\mathbf{r}_{mn}}\Psi_0^2(\mathbf{r}_1,\ldots,\mathbf{r}_N)d^3r_1\cdots d^3r_N\ . \tag{2.17}$$

In Eq. (2.16), m is summed from 1 to N and n from 1′ to N, while in Eq. (2.17) for X_k both m and n are summed from 1 to N.

There are N terms with $m=n$ in X_k, and their contribution is NX_0. The $m\neq n$ terms are calculated by cluster expansion. As in the theory of elementary excitations, the $\exp(i\mathbf{k}\cdot\mathbf{r}_{mn})$ is represented in the cluster diagrams by an exchange line from m to n. The sum of irreducible diagrams containing this line is denoted by $[B]$. The ratio X_k/X_0 is easily calculated to be

$$X_k/X_0=N+[B]=NS(k)\ , \tag{2.18}$$

where $S(k)$ is the familiar static structure function. Since this ratio is of order N, we have to calculate the U_k in Eq. (2.15) to order 1.

The contribution of terms with $m=n$ to Y_k is $(N-1)Y_0$, and to U_k is $-n_0(\mathbf{r}_{11'})$. The contribution of $m\neq n$ terms has to be calculated with cluster expansion. The $m\neq n$ terms of Y_k can be written as

$$Y_k(m\neq n)=\rho\{[L]+[L][i]+\tfrac{1}{2}[L][i][j]+\cdots+[I][J]+[I][J][i]+\cdots\}\ , \tag{2.19}$$

where L denotes connected diagrams that contain points 1 and 1′ and the line mn, while J denotes connected diagrams that contain the line mn but not the points 1 and 1′. The ratio is found to be

$$Y_k(m\neq n)/X_0=\rho\{[L]-\overbrace{[L][i]}+\overbrace{[L][i][j]}+\tfrac{1}{2}[\overbrace{\overbrace{L][i][j]}}+\overbrace{[L][i][j]}+\cdots+[I][J]-\overbrace{[I][J][i]}-[I]\overbrace{[J][i]}-\overbrace{[I][J][i]}+\cdots\}\ . \tag{2.20}$$

We also obtain

$$Y_0X_k(m\neq n)/(X_0)^2=\rho\{[I][J]+\overbrace{[I][J]}-[I]\overbrace{[J][i]}-\overbrace{[I][J][i]}-2\overbrace{[I][J][i]}-\overbrace{[I][J][i]}-\overbrace{[I][J][i]}-2\overbrace{[I][J][i]}+\cdots\}\ . \tag{2.21}$$

and thus,

$$U_k(m\neq n)=\rho\{[L]-\overbrace{[L][i]}+\cdots-\overbrace{[I][J]}+\overbrace{[I][J][i]}+\overbrace{[I][J][i]}+\overbrace{[I][J][i]}+2\overbrace{[I][J][i]}+\cdots\}\ . \tag{2.22}$$

Let C denote irreducible diagrams containing points 1 and 1′ and the exchange line mn. We then have

$$[L]=[C]+\overbrace{[Ca']}+\tfrac{1}{2}\overbrace{[Ca'b']}+\tfrac{1}{2}\overbrace{[Ca'b']}+\overbrace{[Ca'b]}+\cdots+\overbrace{[AB']}+\overbrace{[AB'a']}+\overbrace{[AB'a']}+\overbrace{[AB'a]}+\overbrace{[ABa']}+\cdots\ , \tag{2.23}$$

$$[J]=[B]+[Ba]+\cdots\ . \tag{2.24}$$

The irreducible B' diagrams are identical to the B diagrams when they do not contain points 1 or 1′. B' diagrams containing 1 or 1′ have ζ-line starting from 1 or 1′. Substituting Eqs. (2.8), (2.9), (2.23), and (2.24) in (2.22) we obtain

$$\begin{aligned}\frac{1}{\rho}U_k(m\neq n)=&[C]+\{\overbrace{[Ca']}-\overbrace{[C][a]}\}+\cdots+\{\overbrace{[AB']}-\overbrace{[A][B]}\}\\&+\{\overbrace{[AB'a']}-\overbrace{[Aa']}[B]-\overbrace{[A][Ba]}-\overbrace{[AB']}[a]+2\overbrace{[A][B][a]}\}\\&+\{\overbrace{[AB'a']}-\overbrace{[Aa']}[B]-\overbrace{[AB']}[a]+\overbrace{[A][B][a]}\}+\{\overbrace{[AB'a']}-\overbrace{[AB']}[a]-\overbrace{[A][Ba]}+\overbrace{[A][B][a]}\}\\&+\{\overbrace{[ABa']}-\overbrace{[Aa']}[B]-\overbrace{[A][Ba]}+\overbrace{[A][B][a]}\}+\cdots\ .\end{aligned} \tag{2.25}$$

The terms in $\{\ \}$ are nonzero only when the common particles are 1 and/or 1′. All the terms with irreducible diagrams C can be summed up to obtain $[C]\exp(2R_w-R_d)$. One of the $\overbrace{[A][B][a]}$ cancels $\overbrace{[A][Ba]}$, and the $\{\ \}$'s starting from

$[\overline{AB'a}]$ and $[\overline{AB\overline{a}'}]$ give zero contribution because they must have a common particle other than 1 and 1'. The two common particles in the terms of the $\{\ \}$ starting with $[\overline{AB'a'}]$ must be 1 and 1', otherwise this $\{\ \}$ is zero. We denote by B_1, B_1' and $B_{1'}'$ the irreducible diagrams containing particles 1 and 1'. Note that there are no $B_{1'}$ diagrams. The terms in $U_{\mathbf{k}}$ containing A diagrams are reordered in the following two series:

$$-[\overline{A}][\overline{B_1}]-[\overline{Aa_1'}][\overline{B_1}]-[\overline{\overline{Aa}_{1'}'}][\overline{B_1}]+[\overline{A}][\overline{B_1}][\overline{a_1}]+\cdots ,$$

$$+[\overline{AB_1'}]+[\overline{AB_{1'}'}]+[\overline{AB_1'a_1'}]+[\overline{AB_1'a_{1'}'}]+[\overline{\overline{AB}_1'a'_{1'}}]+[\overline{\overline{AB}_1'a_1}]-[\overline{AB_1'}][\overline{a_1}]-[\overline{\overline{AB}_{1'}'}][\overline{a_1}]+\cdots .$$

These series are summed to obtain the total $U_{\mathbf{k}}$ and $\delta n_{\mathbf{k}}(\mathbf{r}_{11'})$ including $m=n$ contribution as

$$U_{\mathbf{k}}=\rho[C]\exp(2R_w-R_d)-n_0(\mathbf{r}_{11'})(1+[B_1]-2[B_1']) , \tag{2.26}$$

$$\delta n_{\mathbf{k}}(\mathbf{r}_{11'})=U_{\mathbf{k}}/[NS(k)] . \tag{2.27}$$

The second term of Eq. (2.26) represents particles taken out of the $n_0(p)$ by the excitation. The structure of $1+[B_1]$ is shown in Fig. 1. We use the diagrammatic notation of Ref. 4 in which dashed and wiggly lines represent generalized $g_{dd}-1$ and $g_{wd}-1$ bonds. These bonds, respectively, represent sums of all possible correlations with h-lines at both ends and with h-lines at one end and ζ-lines at the other. The B_1 diagrams have only $g_{dd}-1$ bonds. From Fig. 1 we obtain

$$1+[B_1]=S^2(k)[1+\Lambda_d(k)] , \tag{2.28}$$

$$\Lambda_d(k)=\rho^2\int d^3r_{12}d^3r_{13}e^{i\mathbf{k}\cdot\mathbf{r}_{23}}[g_{dd}(12)-1][g_{dd}(13)-1][g_{dd}(23)-1]$$
$$\times(1+A_{ddd}(123)\{1+[g_{dd}(12)-1]^{-1}+[g_{dd}(13)-1]^{-1}+[g_{dd}(23)-1]^{-1}\}) , \tag{2.29}$$

where $A_{ddd}(123)$ is the contribution of Abe diagrams.

The $[B_1']$ is shown in Fig. 2. We obtain

$$[B_1']=[B_{1'}']=g_{wd}(k)[1+g_{wd}(k)]+S^2(k)\Lambda_w(k) , \tag{2.30}$$

$$g_{wd}(k)=\rho\int d^3r[g_{wd}(r)-1]e^{i\mathbf{k}\cdot\mathbf{r}} , \tag{2.31}$$

$$\Lambda_w(k)=\rho^2\int d^3r_{12}d^3r_{13}e^{i\mathbf{k}\cdot\mathbf{r}_{23}}[g_{wd}(12)-1][g_{wd}(13)-1][g_{dd}(23)-1]$$
$$\times(1+A_{wwd}(123)\{1+[g_{wd}(12)-1]^{-1}+[g_{wd}(13)-1]^{-1}+[g_{dd}(23)-1]^{-1}\}) . \tag{2.32}$$

We define $t_1(k)$ as

$$t_1(k)=(2[B_1']-1-[B_1])/S(k)=\frac{2}{S(k)}g_{wd}(k)[1+g_{wd}(k)]-S(k)[1+\Lambda_d(k)-2\Lambda_w(k)] , \tag{2.33}$$

so that the contribution of this term to $\delta n_{\mathbf{k}}(\mathbf{r}_{11'})$ is simply $t_1(k)n_0(r_{11'})/N$.

The contribution of C diagrams [Eq. (2.26)] can be divided into three parts. The diagrams belonging to the first part are shown in Fig. 3(a), and their contribution is given by

$$\frac{1}{NS(k)}n_0(r_{11'})e^{i\mathbf{k}\cdot\mathbf{r}_{11'}}[1+g_{wd}(k)]^2\equiv\frac{1}{N}t_2(k)n_0(\mathbf{r}_{11'})e^{i\mathbf{k}\cdot\mathbf{r}_{11'}} . \tag{2.34}$$

The contribution of diagrams included in the second part [Fig. 3(b)] is obtained as

$$\frac{1}{NS(k)}n_0(r_{11'})e^{-i\mathbf{k}\cdot\mathbf{r}_{11'}}[g_{wd}(k)]^2\equiv\frac{1}{N}t_3(k)n_0(r_{11'})e^{-i\mathbf{k}\cdot\mathbf{r}_{11'}} . \tag{2.35}$$

The third part includes all other C diagrams, whose contribution depends upon the directions of $\mathbf{k}$ and $\mathbf{r}_{11'}$ in a nontrivial fashion. We express it as $T(\mathbf{k},\mathbf{r}_{11'})n_0(r_{11'})/N$,

$$T(\mathbf{k},\mathbf{r}_{11'})=[1+g_{wd}(k)]D(\mathbf{k},\mathbf{r}_{11'})+g_{wd}(k)D^*(\mathbf{k},\mathbf{r}_{11'})+S(k)D'(\mathbf{k},\mathbf{r}_{11'}) . \tag{2.36}$$

The $D(\mathbf{k},\mathbf{r}_{11'})$ term is from diagrams shown in Fig. 4(a), while the second $D^*(\mathbf{k},\mathbf{r}_{11'})$ term is from diagrams of Fig. 4(b). We have

$$D(\mathbf{k},\mathbf{r}_{11'})=\rho\int d^3r_{12}(e^{i\mathbf{k}\cdot\mathbf{r}_{12}}+e^{i\mathbf{k}\cdot\mathbf{r}_{21'}})[g_{wd}(12)-1][g_{wd}(1'2)-1]$$
$$\times(1+A_{wwd}(11'2)\{1+[g_{wd}(12)-1]^{-1}+[g_{wd}(1'2)-1]^{-1}\}) . \tag{2.37}$$

The $D'(\mathbf{k},\mathbf{r}_{11'})$ term represents the contribution of four-point and higher-order diagrams shown in Fig. 5.

In all, we have

$$\delta n_{\mathbf{k}}(\mathbf{r}_{11'})=\frac{1}{N}n_0(r_{11'})[t_1(k)+t_2(k)e^{i\mathbf{k}\cdot\mathbf{r}_{11'}}+t_3(k)e^{-i\mathbf{k}\cdot\mathbf{r}_{11'}}+T(\mathbf{k},\mathbf{r}_{11'})] , \tag{2.38}$$

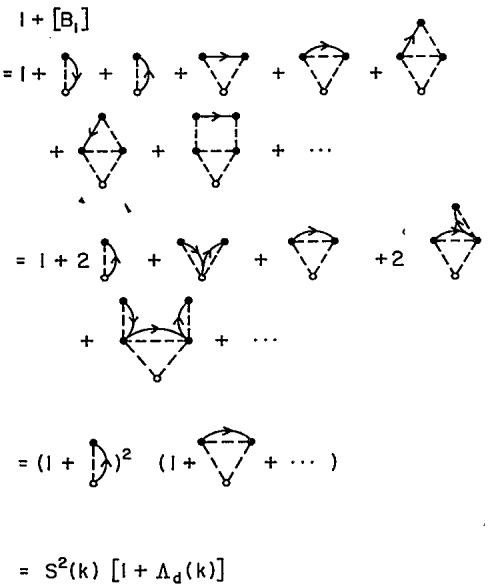

FIG. 1. Diagrammatic calculation of $1+[B_1]$. The dashed lines represent $g_{dd}-1$ bonds, the dots, internal points, and the little circles, the external point 1. The directed line represents the $\exp(i\mathbf{k}\cdot\mathbf{r}_{mm})$.

from which we obtain

$$\delta n_{\mathbf{k}}(\mathbf{p})=\frac{1}{N}[t_1(k)n_0(p)+t_2(k)n_0(|\mathbf{k}-\mathbf{p}|) +t_3(k)n_0(|\mathbf{k}+\mathbf{p}|)+t_4(\mathbf{k},\mathbf{p})] , \quad (2.39)$$

where

$$t_4(\mathbf{k},\mathbf{p})=\int d^3r_{11'}n_0(r_{11'})T(\mathbf{k},\mathbf{r}_{11'})e^{-i\mathbf{p}\cdot\mathbf{r}_{11'}} . \quad (2.40)$$

B. Limiting cases

The $\delta n_{\mathbf{k}}(\mathbf{p})$ takes a rather simple form in the limits $k\to 0$ and $k\to\infty$. At small values of k we have the relations

$$S(k\to 0)=\frac{\hbar}{2mc}k , \quad (2.41)$$

$$g_{wd}(k\to 0)=-\tfrac{1}{2}+\cdots , \quad (2.42)$$

where the ellipsis represents a term of $O(k)$. Here c is the velocity of sound, and the above relations follow from the asymptotic behavior of the pair correlation:[10]

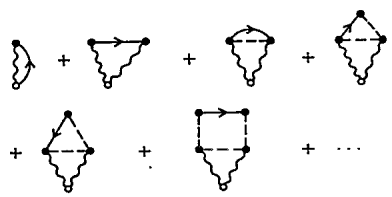

FIG. 2. Diagrams contributing to $[B_1']$. The wiggly lines represent $g_{wd}-1$ bonds, and the small circle denotes point 1. Note that in B_1' diagrams, the exchange lines can start from point 1 but not end in point 1.

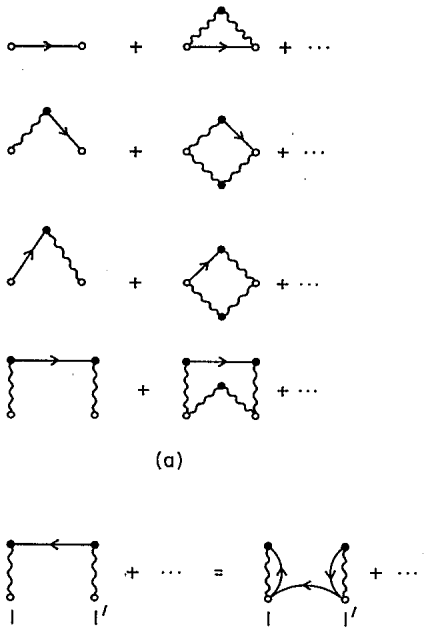

FIG. 3. Diagrams that contribute to t_2 and t_3. The two small circles denote points 1 and 1′. Equations (2.34) and (2.35) are obtained by factorizing the diagrams as illustrated in (b).

$$f(r\to\infty)=1-\frac{mc}{2\pi^2\hbar\rho}\frac{1}{r^2} . \quad (2.43)$$

In the limit $k\to 0$, t_1, t_2, and t_3 have terms of order $1/k$, while T is of order 1, and hence negligible. We find by using the limits (2.41) and (2.42) in Eqs. (2.33)—(2.35)

$$t_1(k\to 0)=-1/[2S(k)] , \quad (2.44)$$

$$t_2(k\to 0)=1/[4S(k)] , \quad (2.45)$$

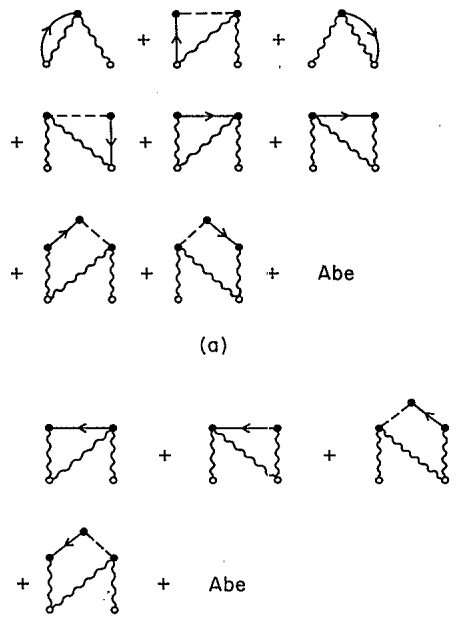

FIG. 4. Diagrams that give $D(\mathbf{k},\mathbf{r}_{11'})$ and $D^*(\mathbf{k},\mathbf{r}_{11'})$ contributions.

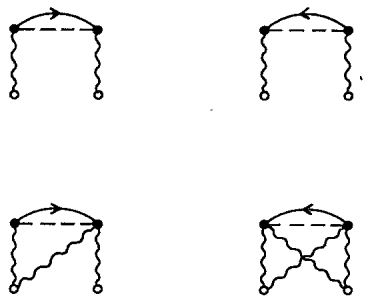

FIG. 5. Some of the diagrams that contribute to $D'(\mathbf{k},\mathbf{r}_{11'})$.

$$t_3(k\to 0)=1/[4S(k)]\ . \tag{2.46}$$

Thus a long-wavelength phonon removes $1/[2S(k)]$ particles from the ground state $n_0(p)$ and divides them equally into two distributions $n_0(|\mathbf{p}-\mathbf{k}|)$ and $n_0(|\mathbf{p}+\mathbf{k}|)$ centered at $\mathbf{p}=\mathbf{k}$ and $\mathbf{p}=-\mathbf{k}$. The $n_0(p)$ has the singular term $Nn_c\delta_{p,0}$, and hence a phonon state has $n_c/[4S(k)]$ particles each in the states with $\mathbf{p}=\pm\mathbf{k}$. The change in the kinetic energy (KE) of the liquid on exciting a phonon is given by

$$\delta(\mathrm{KE})=\frac{\Omega}{(2\pi)^3}\frac{\hbar^2}{2m}\int d^3p\,\delta n_{\mathbf{k}}(\mathbf{p})p^2\ , \tag{2.47}$$

and in the long-wavelength limit it is

$$\delta(\mathrm{KE})(k\to 0)=\frac{\hbar^2k^2}{2m}\frac{1}{2S(k)}=\tfrac{1}{2}\hbar\omega(k)\ . \tag{2.48}$$

The phonon in Bose liquids is, indeed, a pure harmonic vibration with half of its energy from kinetic and the other half from potential terms.

The $k\to\infty$ limit is only of mathematical interest, since we do not expect the Feynman wave function of the excitation to be realistic in this limit. In this limit the excitation has a single-particle character. The $S(k\to\infty)=1$, and $g_{wd}(k\to\infty)$, $\Lambda(k\to\infty)$, and $T(\mathbf{k}\to\infty,\mathbf{r})$ are all zero. Thus, we have

$$t_1(k\to\infty)=-1\ , \tag{2.49}$$

$$t_2(k\to\infty)=1\ , \tag{2.50}$$

$$t_3(k\to\infty)=t_4(\mathbf{k}\to\infty,\mathbf{p})=0\ , \tag{2.51}$$

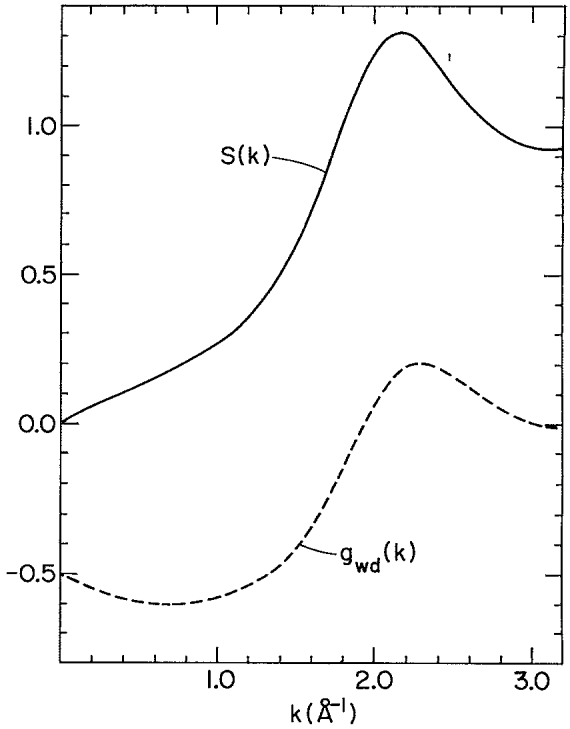

FIG. 6. $S(k)$ and $g_{wd}(k)$.

a single particle is removed from the ground state, and put in a distribution $n_0(|\mathbf{p}-\mathbf{k}|)$ centered at $\mathbf{p}=\mathbf{k}$. In this limit the energy of the Feynman excitation is $\hbar^2k^2/2m$, and it equals the change in the kinetic energy.

C. HNC/S calculations

The pair functions g_{xy}, $xy=dd$, and wd, and the Abe functions A_{xyz}, $xyz=ddd$, ddw, and wwd have been calculated in Ref. 4 with the hypernetted-chain-scaling (HNC/S) method in which the contribution of elementary diagrams is approximated by scaling that of the four-point diagrams. We use these functions to calculate the $\delta n_{\mathbf{k}}(\mathbf{p})$. The $S(k)$ and $g_{wd}(k)$ are shown in Fig. 6 for easy reference. The $g_{dd}(r)$ and $g_{wd}(r)$ are shown in Fig. 2 of Ref. 4. The quantities t_1, t_2, and t_3 are relatively simple integrals of the g and A functions. We find that the $\Lambda_d-2\Lambda_w$ term contributes less than 5% of the t_1, and

TABLE I. Calculated values of the t_i's.

k	$t_1(k)$	$t_2(k)$	$t_3(k)$	$t_{4n}(k)$	$t_{4m}(k)$
0.2	−8.66	3.54	5.21	−0.12	2.15
0.4	−4.68	1.63	3.17	−0.18	2.04
0.6	−3.37	1.08	2.35	−0.13	1.86
0.8	−2.61	0.80	1.75	−0.02	1.63
1.0	−2.12	0.67	1.25	0.14	1.37
1.2	−1.77	0.59	0.81	0.31	1.08
1.4	−1.53	0.56	0.44	0.46	0.78
1.6	−1.39	0.60	0.17	0.53	0.51
1.8	−1.31	0.73	0.02	0.44	0.27
2.0	−1.18	0.92	0.00	0.31	0.16
2.2	−1.00	1.09	0.03	−0.22	−0.06
2.4	−0.87	1.16	0.03	−0.40	−0.13

hence the Abe corrections to the Λ's [Eqs. (2.29) and (2.32)] are neglected. The calculated values of the t_i's are tabulated in Table I.

The $t_4(\mathbf{k},\mathbf{p})$ is generally a function of k, p, and the angle between $\mathbf{k}$ and $\mathbf{p}$. It is difficult to calculate it, but it may be reasonably approximated as follows. We define

$$D_1(\mathbf{k},\mathbf{p})=\int d^3r_{11'}n_0(r_{11'})D(\mathbf{k},\mathbf{r}_{11'})e^{-i\mathbf{p}\cdot\mathbf{r}_{11'}} . \tag{2.52}$$

This integral appears in the contribution of the $D(\mathbf{k},\mathbf{r}_{11'})$ term to $t_4(\mathbf{k},\mathbf{p})$. We can rewrite it as

$$D_1(\mathbf{k},\mathbf{p})=\rho\int d^3r_{11'}n_0(r_{11'})e^{-i(\mathbf{p}-\mathbf{k}/2)\cdot\mathbf{r}_{11'}}\int d^3r_{12}(e^{i\mathbf{k}\cdot\mathbf{r}_{c2}}+e^{-i\mathbf{k}\cdot\mathbf{r}_{c2}})[g_{wd}(12)-1][g_{wd}(1'2)-1](1+\mathscr{A}) , \tag{2.53}$$

where $\mathscr{A}$ represents Abe terms, and

$$\mathbf{r}_c=\tfrac{1}{2}(\mathbf{r}_1+\mathbf{r}_{1'}) . \tag{2.54}$$

It is now clear that $D_1(\mathbf{k},\mathbf{p})$ is invariant under the transformation $\mathbf{p}\to\mathbf{k}-\mathbf{p}$, and hence it is convenient to consider D_1 as a function of k, $|\mathbf{p}-\mathbf{k}/2|$ and the polar angle Θ of $|\mathbf{p}-\mathbf{k}/2|$ using $\mathbf{k}$ to define the Z axis. This function is invariant under the transformation $\Theta\to\pi-\Theta$. We neglected the Abe terms in D, and calculated $D_1(k,|\mathbf{p}-\mathbf{k}/2|,\Theta)$ for chosen values of k, $|\mathbf{p}-\mathbf{k}/2|$, and Θ. The $D_1(k,|\mathbf{p}-\mathbf{k}/2|,\Theta)$ is peaked at $|\mathbf{p}-\mathbf{k}/2|=0$. At small values of $|\mathbf{p}-k/2|$ it has negligible dependence on Θ. For $k=1$ Å^{-1} and $|\mathbf{p}-\mathbf{k}/2|=1$ Å^{-1}, the dependence on Θ is $\sim 15\%$. The D_1 at $k=1$ Å^{-1} has decreased to $\sim$ half its peak value at $|\mathbf{p}-\mathbf{k}/2|=1$ Å^{-1}. Thus it appears that in the first approximation we may neglect the Θ dependence of D_1.

The angle average value,

$$\bar{D}_1(k,|\mathbf{p}-\mathbf{k}/2|)=\tfrac{1}{2}\int_{-1}^{1}d\cos\Theta\, D_1(k,|\mathbf{p}-\mathbf{k}/2|,\Theta) , \tag{2.55}$$

is much simpler to calculate. It is given by

$$\bar{D}_1(k,|\mathbf{p}-\mathbf{k}/2|)=2\rho\int d^3r_{11'}n_0(r_{11'})j_0(|\mathbf{p}-\mathbf{k}/2|r_{11'})\int d^3r_{12}j_0(kr_{c2})[g_{wd}(12)-1][g_{wd}(1'2)-1](1+\mathscr{A}) , \tag{2.56}$$

and should be a good approximation to $D_1(k,|\mathbf{p}-\mathbf{k}/2|,\Theta)$. The results for $k=0.6$, 1.0, and 2.0 Å^{-1} are shown in Fig. 7. This function does not have any singularities. The singularities in $n_0(p)$ come from the long-range ($r_{11'}\to\infty$) part of $n_0(r_{11'})$, which is cut out in the D by the product of short-range functions $g_{wd}(12)-1$ and $g_{wd}(1'2)-1$.

The second integral in the $t_4(\mathbf{k},\mathbf{p})$ involving $D^*(\mathbf{k},\mathbf{r}_{11'})$ is calculated in a similar way. It is easy to show that

$$\int d^3r_{11'}n_0(r_{11'})D^*(k,r_{11'})e^{-i\mathbf{p}\cdot\mathbf{r}_{11'}}=D_1(\mathbf{k},-\mathbf{p})\approx\bar{D}_1(k,|\mathbf{p}+\mathbf{k}/2|) . \tag{2.57}$$

The contribution of $D'(\mathbf{k},\mathbf{r}_{11'})$ contains the integral

$$D_2(\mathbf{k},\mathbf{p})=\int d^3r_{11'}n_0(r_{11'})D'(\mathbf{k},\mathbf{r}_{11'})e^{-i\mathbf{p}\cdot\mathbf{r}_{11'}} . \tag{2.58}$$

It depends upon the polar angle Θ_p of p; however, it is invariant under the transformation $\Theta_p\to\pi-\Theta_p$. We neglect the dependence on Θ_p and approximate D_2 by its angle average

$$\bar{D}_2(k,p)=\tfrac{1}{2}\int_{-1}^{1}d\cos\Theta_p D_2(k,p,\Theta_p) . \tag{2.59}$$

The Abe corrections to D' are neglected; we then have (from Fig. 5):

$$\begin{aligned}\bar{D}_2(k,p)=\rho^2\int d^3r_{11'}n_0(r_{11'})j_0(pr_{11'})\int d^3r_{12}d^3r_{13}j_0(kr_{23})\\ \times(2[g_{wd}(12)-1][g_{wd}(1'3)-1]\{1+[g_{wd}(1'2)-1]+[g_{wd}(13)-1]\}[g_{dd}(23)-1]\\ +[g_{wd}(12)-1][g_{wd}(1'2)-1][g_{wd}(13)-1][g_{wd}(1'3)-1]g_{dd}(23)) .\end{aligned} \tag{2.60}$$

The calculated values are shown in Fig. 8. The $T_4(\mathbf{k},\mathbf{p})$ is thus approximated with

$$\begin{aligned}t_4(\mathbf{k},\mathbf{p})=[1+g_{wd}(k)]\bar{D}_1(k,|\mathbf{p}-\mathbf{k}/2|)\\ +g_{wd}(k)\bar{D}_1(k,|\mathbf{p}+\mathbf{k}/2|)+S(k)\bar{D}_2(k,p) .\end{aligned} \tag{2.61}$$

The $T_4(k=1\text{ Å}^{-1},p,\Theta_p=0)$ is shown in Fig. 9.

The conservation of particles and momentum requires that

$$\frac{\Omega}{(2\pi)^3}\int d^3p\,\delta n_{\mathbf{k}}(\mathbf{p})=0 , \tag{2.63}$$

$$\frac{\Omega}{(2\pi)^3}\int d^3p\,\delta n_{\mathbf{k}}(\mathbf{p})\mathbf{p}=\mathbf{k} . \tag{2.64}$$

This implies that

$$t_1(k)+t_2(k)+t_3(k)+t_{4n}(k)=0 , \tag{2.65}$$

$$t_2(k)-t_3(k)+t_{4m}(k)=1 , \tag{2.66}$$

where

$$t_{4n}(k)=\frac{1}{\rho(2\pi)^3}\int d^3pt_4(k,p,\Theta_p) , \tag{2.67}$$

$$t_{4m}(k)=\frac{1}{\rho(2\pi)^3}\frac{1}{k}\int d^3pt_4(k,p,\Theta_p)p\cos\Theta_p . \tag{2.68}$$

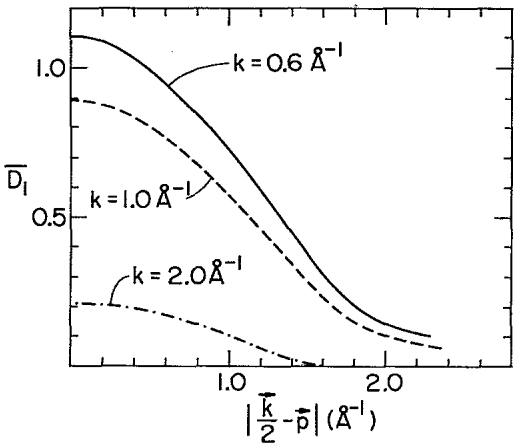

FIG. 7. $\overline{D}_1(k,|\mathbf{k}/2-\mathbf{p}|)$.

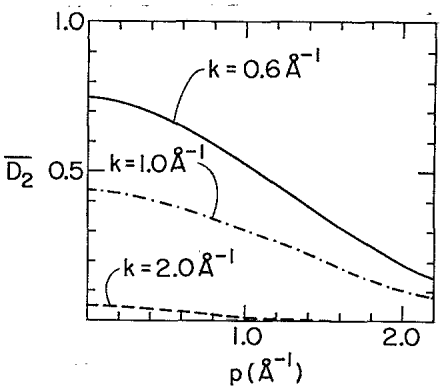

FIG. 8. $\overline{D}_2(k,p)$.

The calculated values of the t's are listed in Table I. The identities 2.65 and 2.66 are satisfied with an accuracy of $\sim 15\%$ of the largest t.

III. THREE-BODY CORRELATIONS

In this section we calculate the $\delta n_{\mathbf{k}}(\mathbf{p})$ with the wave function (1.2) for the ground state and the Feynman excitation operator (1.4), using the three-body correlation determined in Ref. 11. The cluster expansion for the $\delta n_{\mathbf{k}}(\mathbf{p})$ has the form given in Sec. II A; however, we must now consider three-body bonds of the type $[f_3(ijk)]^2-1$ and $f_3(1jk)-1$. The effect of these bonds on the two-point functions $g_{xy}-1$ is taken into account as discussed in Refs. 4 and 11. Their effect on the Abe functions is generally given by

$$A_{wwd}(11'2)=A^g_{wwd}(11'2)+A^t_{wwd}(11'2)\,, \tag{3.1}$$

$$A_{wdd}(123)=f_3(123)[1+A^g_{wdd}(123)+A^t_{wdd}(123)]-1\,, \tag{3.2}$$

$$A_{ddd}(123)=[f_3(123)]^2[1+A^g_{ddd}(123)+A^t_{ddd}(123)]-1\,, \tag{3.3}$$

where A^g_{xyz} are four- or more-body Abe corrections from two-body bonds $g_{xy}-1$, and A^t_{xyz} are four- or more-body Abe corrections that include three-body bonds.

The t_2 and t_3 [Eqs. (2.34) and (2.35)] contain only two-body integrals, and they are calculated as described in the last section. In the Jastrow calculations and here also we neglect all Abe corrections to the Λ's [Eqs. (2.29) and (2.32)]. This corresponds to the following approximations for the Λ's:

$$\Lambda_d(k)=\rho^2\int d^3r_{12}d^3r_{12}d^3r_{13}e^{i\mathbf{k}\cdot\mathbf{r}_{23}}([g_{dd}(12)-1][g_{dd}(23)-1][g_{dd}(31)-1]+\{[f_3(123)]^2-1\}g_{dd}(12)g_{dd}(23)g_{dd}(31))\,, \tag{3.4}$$

$$\Lambda_w(k)=\rho^2\int d^3r_{12}d^3r_{13}e^{i\mathbf{k}\cdot\mathbf{r}_{23}}\{[g_{wd}(12)-1][g_{wd}(13)-1][g_{dd}(23)-1]+[f_3(123)-1]g_{wd}(12)g_{wd}(13)g_{dd}(23)\}\,. \tag{3.5}$$

The three-body correlations do not have a large effect on the $n_0(p)$ as discussed in Ref. 4. The calculated values of the t_{1-3} with the wave function (1.2) are listed in Table II. These differ from the t_{1-3} for the Jastrow Ψ_0 by $<15\%$. The effect of the triplet correlation on the $t_4(\mathbf{k},\mathbf{p})$ has not been calculated.

IV. BACKFLOW CORRELATIONS

In this section we calculate the t_{1-3} with wave functions (1.2) for the ground state and (1.5) and (1.6) for the excited state. The cluster expansion of Sec. II A is still valid; however, we now have many more terms containing the backflow correlation bonds $\eta(r_{ij})\mathbf{k}\cdot\mathbf{r}_{ij}$. There are no two-body backflow correlations in the ground state, and so the g_{xy} do not contain two-body backflow effects. The triplet correlation, however, can be thought of as a backflow effect.[12]

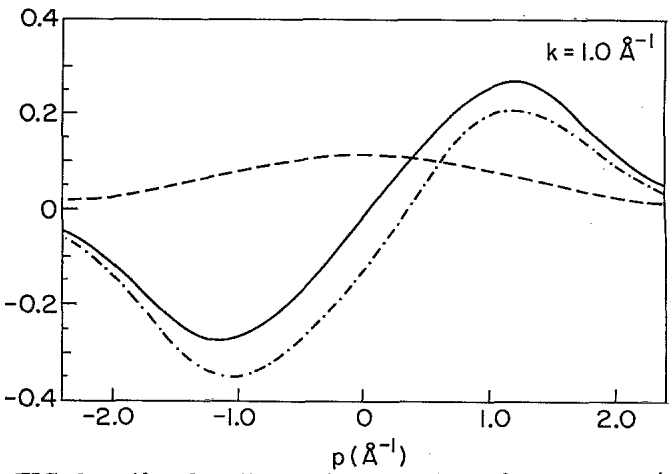

FIG. 9. $t_4(k,p,\Theta_p=0)$. Total contributions of the D and D^* terms is shown by the dashed-dotted line, and the dashed line gives that of the D' term. The full line gives $t_4(k,p,\Theta_p=0)$.

TABLE II. Calculated $t_1(k)$, $t_2(k)$, and $t_3(k)$ using Jastrow (J), Jastrow plus triplet (J + T), and Jastrow plus triplet plus backflow (J + T + B) wave functions.

	$t_1(k)$			$t_2(k)$			$t_3(k)$		
k	J	J+T	J+T+B	J	J+T	J+T+B	J	J+T	J+T+B
0.2	−8.66	−10.02	−9.89	3.54	4.23	4.13	5.21	5.89	5.85
0.4	−4.68	−5.43	−5.17	1.63	2.03	1.82	3.17	3.55	3.44
0.6	−3.37	−3.54	−3.23	1.08	1.20	0.92	2.35	2.44	2.25
0.8	−2.61	−2.49	−2.27	0.80	0.77	0.49	1.75	1.70	1.46
1.0	−2.12	−2.00	−1.93	0.67	0.60	0.35	1.25	1.18	0.96
1.2	−1.77	−1.76	−1.82	0.59	0.56	0.35	0.81	0.77	0.63
1.4	−1.53	−1.61	−1.75	0.56	0.56	0.41	0.44	0.44	0.37
1.6	−1.39	−1.48	−1.63	0.60	0.61	0.52	0.17	0.18	0.16
1.8	−1.31	−1.36	−1.48	0.73	0.73	0.68	0.02	0.03	0.02
2.0	−1.18	−1.17	−1.24	0.92	0.93	0.91	0.00	0.00	0.00
2.2	−1.00	−0.93	−0.96	1.09	1.10	1.10	0.03	0.03	0.03
2.4	−0.87	−0.80	−0.83	1.16	1.17	1.15	0.03	0.03	0.03

We have developed, in Ref. 8, two approximations to sum backflow terms. These approximations must be used with the short-range backflow function $\eta_S(r)$ of Ref. 8. The simpler of these is called the two-body (TB) factorizable approximation in which only those terms whose contributions can be expressed as products of two-body integrals are retained. The second, called extended TB or ETB, considers the modification of the backflow correlation $\eta(r)$ due to Jastrow and triplet correlations in calculating the TB integrals. For the sake of clarity we first calculate the t_{1-3} in the TB approximation, and later give expressions for the ETB.

The ratio $X_{\mathbf{k}}/X_0$, given by $NS(k)$ in the Jastrow theory [Eq. (2.18)], becomes

$$\frac{X_{\mathbf{k}}}{X_0}\equiv\frac{\langle\Psi_0|\rho_B^\dagger(\mathbf{k})\rho_B(\mathbf{k})|\Psi_0\rangle}{\langle\Psi_0|\Psi_0\rangle}\equiv NX_B(k)$$

$$=N\{S(k)[1+\tfrac{1}{2}\bar{I}_{9,2}(k)]^2+\bar{I}_{10,2}(k)\}\ , \tag{4.1}$$

in the TB approximation.[8] The two-body integrals $\bar{I}_{9,2}(k)$ and $I_{10,2}(k)$ are

$$\bar{I}_{9,2}(k)=2\rho\int d^3r e^{i\mathbf{k}\cdot\mathbf{r}}\eta(r)i\mathbf{k}\cdot\mathbf{r}g_{dd}(r)\ , \tag{4.2}$$

$$\bar{I}_{10,2}(k)=\rho\int d^3r(1-e^{i\mathbf{k}\cdot\mathbf{r}})[\mathbf{k}\cdot\mathbf{r}\eta(r)]^2g_{dd}(r)\ . \tag{4.3}$$

We have to replace the $S(k)$ in the denominator of Eq. (2.27) for $\delta n_{\mathbf{k}}(\mathbf{r}_{11'})$ by the $X_B(k)$.

The terms included in this calculation of $X_B(k)$ are illustrated with diagrams in Fig. 10. The dashed-dotted line in these diagrams represents the backflow correlation $i\eta(r)\mathbf{k}\cdot\mathbf{r}$ (in Ref. 8 the backflow correlations are shown by wiggly lines which we have used here for denoting $g_{wd}-1$ bonds). The backflow is around the particle in momentum state $\mathbf{k}$. The exchange line starts and ends on the vertices representing this particle in $\Psi_{\mathbf{k}}$ and $\Psi_{\mathbf{k}}^*$. Thus all backflow correlations in $\Psi_{\mathbf{k}}$ must start from the beginning of the exchange line, while those in $\Psi_{\mathbf{k}}^*$ must start from the end of the exchange line. A mark between the exchange and the backflow line is used to differentiate the backflow correlations from $\Psi_{\mathbf{k}}$ and $\Psi_{\mathbf{k}}^*$. If the mark is at the beginning of the exchange line the correlation is from $\Psi_{\mathbf{k}}$, and if it is at the end then the correlation is from $\Psi_{\mathbf{k}}^*$. The backflow correlation between two points i and j is $\pm i\eta(r_{ij})\mathbf{k}\cdot\mathbf{r}_{ij}$, where i is the vertex at which the lines are marked, and the sign is positive (negative) when it is from $\Psi_{\mathbf{k}}$ ($\Psi_{\mathbf{k}}^*$). We note that in the numerator diagrams with points 1 and 1′, the point 1 can only have backflow correlations from $\Psi_{\mathbf{k}}$, and 1′ from $\Psi_{\mathbf{k}}^*$.

The diagrams of Fig. 11 illustrate the backflow contribution to $[B_1]$ in the TB approximation. The terms of Fig. 11.1 give $S_B(k)\bar{I}_{9,2}(k)$, where

$$S_B(k)=S(k)[1+\tfrac{1}{2}\bar{I}_{9,2}(k)]\ . \tag{4.4}$$

The terms of Fig. 11.2 give

$$S^2(k)\{\bar{I}_{9,2}(k)+\tfrac{1}{4}[\bar{I}_{9,2}(k)]^2\}\ , \tag{4.5}$$

to which we add $S^2(k)$ from the contribution with no backflow lines [Eq. (2.28)] to obtain $[S_B(k)]^2$. The terms of Fig. 11.3 give $2\bar{I}_{10,2}(k)$, while those of Fig. 11.4 together with the $S^2(k)\Lambda_d(k)$ from Eq. (2.28) give $[S_B(k)]^2\Lambda_d(k)$. Thus the $1+[B_1]$ in TB approximation is given by

$$1+[B_1]=S_B(k)\bar{I}_{9,2}(k)+S_B^2(k)[1+\Lambda_d(k)]+2\bar{I}_{10,2}(k)\ . \tag{4.6}$$

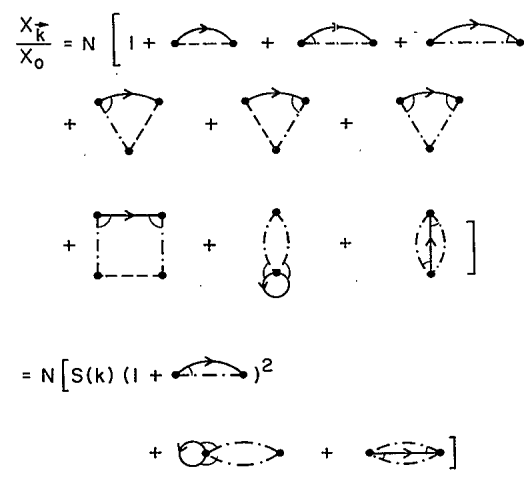

FIG. 10. Diagrammatic illustration of the calculation of X_k/X_0 in the TB approximation.

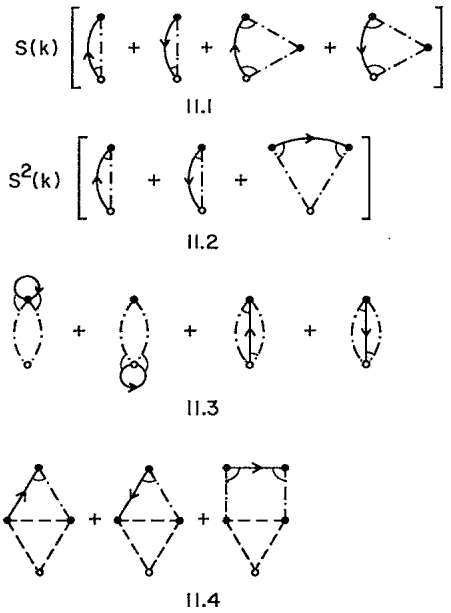

FIG. 11. Backflow diagrams in $[B_1]$.

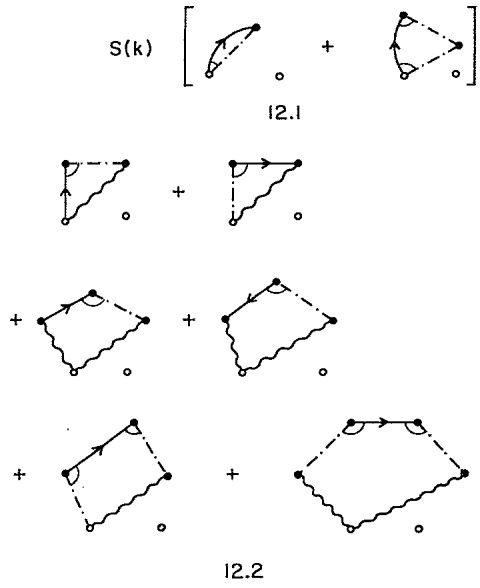

FIG. 12. Backflow diagrams in $[B_1']$.

The backflow contribution to $[B_1']$ is illustrated in Fig. 12. The diagrams of Fig. 12.1 give $\frac{1}{2}S_B(k)\bar{I}_{wd,2}(k)$, where

$$\bar{I}_{wd,2}(k)=2\rho\int i\mathbf{k}\cdot\mathbf{r}\eta(r)g_{wd}(r)e^{i\mathbf{k}\cdot\mathbf{r}}d^3r\ . \tag{4.7}$$

On adding the contribution of diagrams 12.2 to the $g_{wd}(k)[1+g_{wd}(k)]$ from Eq. (2.30) we obtain

$$g_{wd}(k)[1+\tfrac{1}{2}\bar{I}_{9,2}(k)]\times\{1+g_{wd}(k)[1+\tfrac{1}{2}\bar{I}_{9,2}(k)]+\tfrac{1}{2}\bar{I}_{dw,2}(k)\}\ . \tag{4.8}$$

In the TB approximation $\bar{I}_{dw,2}=\bar{I}_{wd,2}$ [Eq. (4.7)]. Diagrams of Fig. 11.4, with wiggly instead of the dashed lines from point 1, also contribute to $[B_1']$. They convert the $S^2(k)\Lambda_w(k)$ of Eq. (2.30) to $[S_B(k)]^2\Lambda_w(k)$. In all we obtain

$$t_1(k)=\frac{1}{X_B(k)}(2g_{wd}(k)[1+\tfrac{1}{2}\bar{I}_{9,2}(k)]\{1+g_{wd}(k)[1+\tfrac{1}{2}\bar{I}_{9,2}(k)]+\tfrac{1}{2}\bar{I}_{dw,2}(k)\}$$
$$+S_B(k)[\bar{I}_{wd,2}(k)-\bar{I}_{9,2}(k)]-S_B^2(k)[1+\Lambda_d(k)-2\Lambda_w(k)]-2\bar{I}_{10,2}(k))\ . \tag{4.9}$$

The backflow $[C]$ diagrams that contribute to t_2 are shown in Fig. 13. By adding their contribution to that of diagrams without backflow lines [Eq. (2.34)] we obtain

$$t_2(k)=\frac{1}{X_B(k)}\{1+g_{wd}(k)[1+\tfrac{1}{2}\bar{I}_{9,2}(k)]+\tfrac{1}{2}\bar{I}_{dw,2}\}^2\ . \tag{4.10}$$

Similarly by adding the contribution of $[C]$ diagrams in Fig. 14 to the t_3 of Eq. (2.35), we get

$$t_3(k)=\frac{1}{X_B(k)}\{g_{wd}(k)[1+\tfrac{1}{2}\bar{I}_{9,2}(k)]\}^2\ . \tag{4.11}$$

In the ETB approximation we add the contribution of diagrams with elements shown in Fig. 15.1 to all diagrams that contain the element shown in Fig. 15.2. The contribution of the elements of Fig. 15.1 is denoted by $\delta\eta_{dd}(r)$:

$$\delta\eta_{dd}(r_{ij})=\frac{\rho}{r_{ij}^2}\int d^3r_{ik}\,\mathbf{r}_{ij}\cdot\mathbf{r}_{ik}\eta(r_{ik})g_{dd}(ik)\times[g_{dd}(jk)-1-\mathscr{A}]\ . \tag{4.12}$$

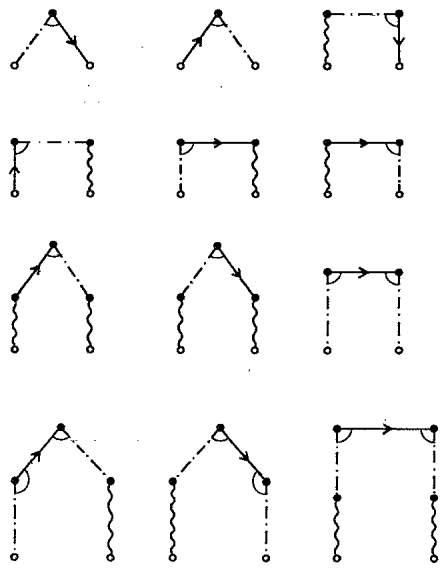

FIG. 13. Backflow diagrams contributing to t_2.

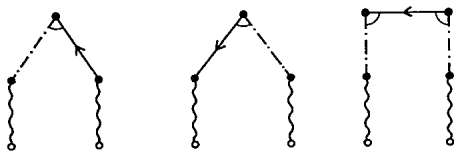

FIG. 14. Backflow diagrams contributing to t_3.

The elements $\delta\eta_{dw}(r)$ and $\delta\eta_{wd}(r)$ are shown in Figs. 15.3 and 15.5 We obtain

$$\delta\eta_{dw}(r_{i1})=\frac{\rho}{r_{il}^2}\int d^3r_{ik}\mathbf{r}_{il}\cdot\mathbf{r}_{ik}\eta(r_{ik})g_{dd}(ik)\times[g_{wd}(lk)-1+\mathscr{A}]\,, \tag{4.13}$$

$$\delta\eta_{wd}(r_{li})=\frac{\rho}{r_{li}^2}\int d^3r_{lk}\mathbf{r}_{lk}\cdot\mathbf{r}_{li}\eta(r_{lk})g_{wd}(r_{lk})\times[g_{dd}(ik)-1+\mathscr{A}]\,. \tag{4.14}$$

These are added to diagrams that have elements in Figs. 15.4 and 15.6, respectively.

The two-body integrals $\bar{I}_{9,2}(k)$, $\bar{I}_{wd,2}(k)$, $\bar{I}_{dw,2}(k)$, $\bar{I}_{10,2}(k)$ modified by the $\delta\eta$ contributions are, respectively, given by

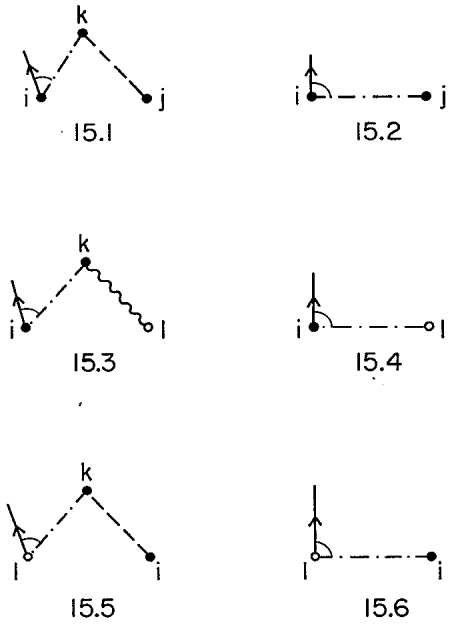

FIG. 15. Elements 15.1, 15.3, and 15.5 represent the $\delta\eta$'s. They can substitute the η elements 15.2, 15.4, and 15.6 in TB diagrams. The exchange lines in elements 15.1, 15.2, and 15.3 can have any direction.

$$\bar{I}_9(k)=2\rho\int d^3r\; i\mathbf{k}\cdot\mathbf{r}e^{i\mathbf{k}\cdot\mathbf{r}}\{\eta(r)g_{dd}(r)+\delta\eta_{dd}(r)[g_{dd}(r)-1]\}\,, \tag{4.15}$$

$$\bar{I}_{wd}(k)=2\rho\int d^3r\; i\mathbf{k}\cdot\mathbf{r}e^{i\mathbf{k}\cdot\mathbf{r}}\{\eta(r)g_{wd}(r)+\delta\eta_{wd}(r)[g_{wd}(r)-1]\}\,, \tag{4.16}$$

$$\bar{I}_{dw}(k)=2\rho\int d^3r\; i\mathbf{k}\cdot\mathbf{r}e^{i\mathbf{k}\cdot\mathbf{r}}\{\eta(r)g_{wd}(r)+\delta\eta_{dw}(r)[g_{wd}(r)-1]\}\,, \tag{4.17}$$

$$\bar{I}_{10}(k)=\rho\int d^3r\; g_{dd}(r)(\mathbf{k}\cdot\mathbf{r})^2\{\eta(r)[\eta(r)+\delta\eta_{dd}(r)]-e^{i\mathbf{k}\cdot\mathbf{r}}[\eta(r)+\delta\eta_{dd}(r)]^2\}\,. \tag{4.18}$$

The calculated values of t_{1-3} in the ETB approximation are listed in Table II. We see that the backflow correlations have a significant effect on the t_2 in the maxon region ($k\sim1$ Å^{-1}). We have not calculated the effect to backflow correlations on $t_4(\mathbf{k},\mathbf{p})$.

V. MOMENTUM DISTRIBUTION AT LOW TEMPERATURES

At low (<1 K) temperatures liquid ^{4}He can be thought of as a gas of noninteracting elementary excitations. Thus the momentum distribution of atoms in the liquid at low temperatures can be expressed as

$$n(T,p)=n_0(p)+\delta n(T,p)\,, \tag{5.1}$$

$$\delta n(T,p)=\frac{\Omega}{(2\pi)^3}\int\frac{d^3k}{\exp[\beta\epsilon(k)]-1}\delta n_{\mathbf{k}}(\mathbf{p})\,, \tag{5.2}$$

where $\epsilon(k)$ is the energy of the excitation of momentum k, and β is the inverse temperature. In this temperature range only the excitations with $k<0.2$ Å^{-1} are important, and the t_4 term of the $\delta n_{\mathbf{k}}(\mathbf{p})$ is unimportant. Neglecting it we obtain

$$\delta n(T,p)=\delta n_1(T,p)+\delta n_2(T,p)\,, \tag{5.3}$$

$$\delta n_1(T,P)=\frac{1}{(2\pi)^3\rho}n_0(p)\int\frac{d^3k}{\exp[\beta\epsilon(k)]-1}t_1(k)\,, \tag{5.4}$$

$$\delta n_2(T,p)=\frac{1}{(2\pi)^3\rho}\int\frac{d^3k}{\exp[\beta\epsilon(k)]-1}\times[t_2(k)+t_3(k)]n_0(|\mathbf{p}-\mathbf{k}|)\,. \tag{5.5}$$

TABLE III. Change in the condensate fraction n_c as a function of temperature. The theoretical value (Refs. 2 and 4) at $T=0$ $n_c(0)$ is 0.092 and the experimental value (Ref. 6) is 0.139 ± 0.023.

	$\frac{\delta n_c(T)}{n_c(0)}$		
T	J	J + T	J + T + B
0.1	−0.000 16	−0.000 16	−0.000 16
0.2	−0.000 66	−0.000 64	−0.0064
0.3	−0.0015	−0.0014	−0.0014
0.4	−0.0027	−0.0025	−0.0025
0.5	−0.0041	−0.0039	−0.0039
0.6	−0.0059	−0.0055	−0.0055
0.7	−0.0079	−0.0074	−0.0074
0.8	−0.0103	−0.0095	−0.0095
0.9	−0.0129	−0.0118	−0.0119
1.0	−0.0157	−0.0144	−0.0145

TABLE IV. Change in the momentum distribution $\delta n(p,T)$ for various temperatures. The last column is the momentum distribution in the ground state obtained from variational calculation (Ref. 4).

	$\delta n(p,T)$					
p (Å^{-1}) \ T (K)	0.2	0.4	0.6	0.8	1.0	$n(p,0)$
0.015	2.825	8.919	15.413	22.010	28.646	5.01
0.035	0.195	1.065	2.155	3.312	4.497	2.36
0.055	0.010	0.177	0.504	0.944	1.341	1.66
0.075	0.001	0.053	0.190	0.379	0.595	1.33
0.095	0.000	0.011	0.060	0.146	0.256	1.14
0.115		0.003	0.024	0.070	0.134	1.02
0.135		0.001	0.008	0.030	0.065	0.93
0.155		0.000	0.003	0.014	0.034	0.86
0.175				0.006	0.018	0.81
0.195				0.003	0.009	0.76
0.215				0.001	0.005	0.73
0.235				0.001	0.003	0.70

We can further approximate the $\delta n(T,p)$ at small T by using the small-k limits discussed in Sec. II B. This gives

$$\delta n_1(T,P)=\frac{-1}{(2\pi)^3\rho}n_0(p)\int\frac{d^3k}{\exp(\beta\hbar kc)-1}\frac{mc}{\hbar k}$$

$$=-n_0(\mathbf{p})T^2\left\langle\frac{m}{12\rho\hbar^3c}\right\rangle\equiv-n_0(p)(T/T_0)^2\,, \tag{5.6}$$

$$\delta n_2(T,p)=\frac{1}{(2\pi)^3\rho}\int\frac{d^3k}{\exp(\beta\hbar kc)-1}\frac{mc}{\hbar k}n_0(|\mathbf{k}-\mathbf{p}|)\,. \tag{5.7}$$

The effect of temperature on the fraction of particles n_c in the $p=0$ state is given by Eq. (5.6) as

$$n_c(T)=n_c(T=0)[1-(T/T_0)^2]\,, \tag{5.8}$$

where T_0 is $\sim$7.6 K. The above equation has also been obtained by a phenomenological approach,[13] and from the structure of the perturbation theory at finite temperature.[14] The results for the condensate fraction obtained with the $\epsilon(k)$ and the $t_1(k)$ [Eq. (5.4)] are given in Table III. These are quite close to the asymptotic ($T\to0$) form (5.8), and fairly independent of the choice of the wave functions. They mostly depend upon the experimentally known $S(k)$ and $\epsilon(k)$.

The δ-function term $\rho n_c(0)\delta(p)$ in $n_0(p)$ gives rise to terms in $\delta n_2(T,p)$ that have singular behavior at $p\to0$. We denote by $\delta n_s(T,p)$ the contribution of this term to $\delta n_2(T,p)$:

$$\delta n_s(T,p)=\frac{n_c(0)mc}{\hbar p}\frac{1}{\exp(\beta\hbar pc)-1}\,. \tag{5.9}$$

At small p ($\beta\hbar pc\ll1$) we can expand the Bose factor in powers of p:

$$\frac{1}{\exp(\beta\hbar pc)-1}=\frac{1}{\beta\hbar pc}-\frac{1}{2}+\cdots\,, \tag{5.10}$$

and obtain

$$\delta n_s(T,p)=n_c(0)\frac{m}{\hbar^2\beta p^2}-\tfrac{1}{2}n_c(0)\frac{mc}{\hbar p}+\cdots\,. \tag{5.11}$$

Recall that the $n_0(p)$ has exactly the same $1/p$ term[4] with positive sign. Thus at $\beta p\hbar c\ll1$, the $1/p$ term in the $n_0(p)$ is exactly cancelled by the $1/p$ term in $\delta n(T,P)$. Thus the total $n(T,p)$ can be expected to exhibit the $1/p$ singularity only for $\beta\hbar pc>1$. This cancellation has recently been noted by Griffin.[15] The $1/p^2$ term in Eq. (5.11) has been discussed in Refs. 13 and 14.

The calculated values of the $\delta n(T,p\neq0)$ are shown in Table IV. The Eqs. (5.3)—(5.5) are used to obtain these results, but they are not too sensitive to the deviations of $t_{1-3}(k)$ or $\epsilon(k)$ from their low-k limits. The $\delta n(T,p\neq0)$ is positive in this temperature range. Thus it appears that at low temperatures, atoms are removed from the $p=0$ condensate and put in states with $\epsilon(p)\leq\pi T$. The momentum distribution at values of p such that $\epsilon(p)>\pi T$ is unaffected by the thermal effects.

ACKNOWLEDGMENT

This work was supported by the U. S. Department of Energy, Division of Materials Sciences, under Grant No. DE-AC02-767ER01198.

[1]M. H. Kalos, M. A. Lee, P. A. Whitlock, and G. V. Chester, Phys. Rev. B **24**, 115 (1981).
[2]P. A. Whitlock and R. M. Panoff (unpublished).
[3]M. L. Ristig and J. W. Clark, Phys. Rev. B **14**, 2875 (1976); S. Fantoni, Nuovo Cimento A **44**, 191 (1978); P. M. Lam and M. L. Ristig, Phys. Rev. B **20**, 1960 (1979).
[4]E. Manousakis, V. R. Pandharipande, and Q. N. Usmani, preceding paper, Phys. Rev. B **31**, 7022 (1985).
[5]P. E. Sokol, R. O. Simmons, R. O. Hilleke, and D. L. Price (unpublished).

[6]V. F. Sears, Phys. Rev. B **28**, 5109 (1983). V. F. Sears, E. C. Svensson, P. Martell, and A. B. D. Woods, Phys. Rev. Lett. **49**, 279 (1982).
[7]R. P. Feynman and M. Cohen, Phys. Rev. **102**, 1189 (1956).
[8]E. Manousakis and V. R. Pandharipande, Phys. Rev. B **30**, 5062 (1984).
[9]V. R. Pandharipande and R. B. Wiringa, Rev. Mod. Phys. **51**, 821 (1979).
[10]L. Reatto and G. V. Chester, Phys. Lett. **22**, 276 (1966).
[11]A. N. Usmani, S. Fantoni, and V. R. Pandharipande, Phys. Rev. B **26**, 6123 (1982).
[12]V. R. Pandharipande, Phys. Rev. B **18**, 218 (1978).
[13]R. A. Ferrell, N. Menyhard, H. Schmidt, F. Schwabl, and P. Szepfalusy, Ann. Phys. (N.Y.) **47**, 565 (1968).
[14]K. Kehr, Z. Phys. **221**, 291 (1969).
[15]A. Griffin, Phys. Rev. B **30**, 5057 (1984).